Research Square

Preprints are preliminary reports that have not undergone peer review.
They should not be considered conclusive, used to inform clinical practice,
or referenced by the media as validated information.

Predictive Equilibrium–Flux Framework for Zn(II) Extraction and Stripping with Cyanex 272

Muhammad Saidur Rahman

saeed_hamim@yahoo.com

Pundra University of Science & Technology

Research Article

Keywords: Zinc solvent extraction, Cyanex 272, Stripping kinetics, Single-drop technique, Interfacial reaction, Process design, Predictive modeling, Machine Learning

Posted Date: November 3rd, 2026

DOI: https://doi.org/10.21203/rs.3.rs-11580354/v1

License: This work is licensed under a Creative Commons Attribution 4.0 International License.
Read Full License

Additional Declarations: No competing interests reported.

Predictive Equilibrium–Flux Framework for Zn(II) Extraction and Stripping with Cyanex 272

Muhammad Saidur Rahman*
Associate Professor
Department of Chemistry
Pundra University of Science & Technology, Gokul, Bogura-5800, Bangladesh
ORCID (MSR): 0000-0003-3751-6863
*Corresponding Author: saeed_hamim@yahoo.com

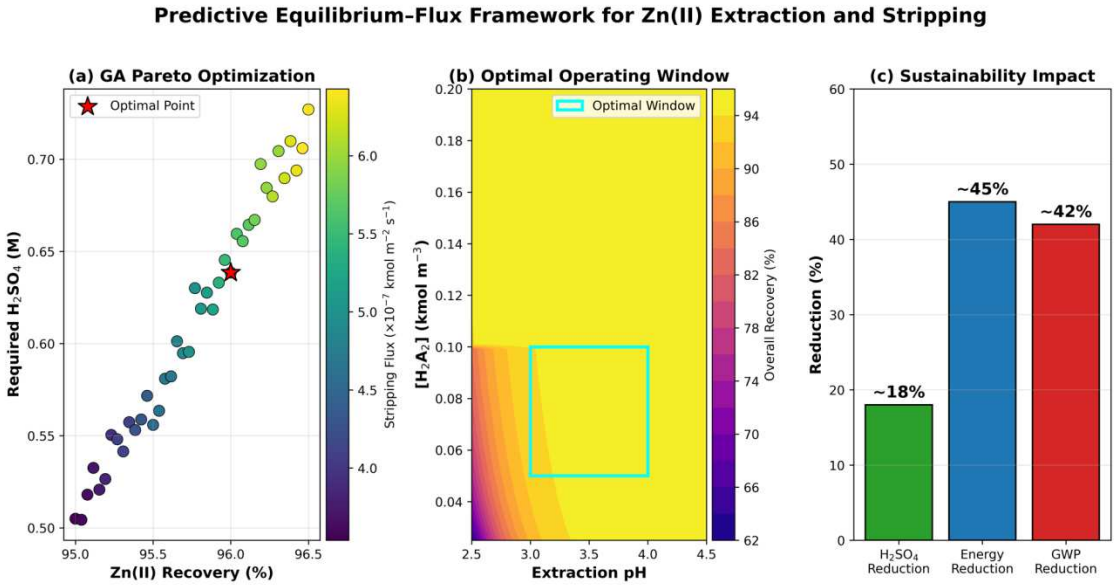
ABSTRACT:

The design and scale-up of hydrometallurgical solvent extraction circuits require quantitative understanding of both equilibrium partitioning and intrinsic stripping kinetics. Although Zn(II) extraction by Cyanex 272 (bis(2,4,4-trimethylpentyl)phosphinic acid) is well documented, hydrodynamics-independent kinetic descriptions of stripping remain unavailable. This work addresses this gap by developing a predictive equilibrium–flux framework for the Zn(II)/Cyanex 272/kerosene/H_2SO_4 system. Equilibrium studies confirm a cation-exchange mechanism (Zn^{2+} + $2HA \rightleftharpoons ZnA_2 + 2H^+$) with second-order pH dependence and exothermic thermodynamics (ΔH = −6.9 to −21.4 kJ mol^{-1}). Sulfuric acid achieves >95% stripping efficiency at ≥0.50 M. The core contribution is the first quantitative flux-based kinetic analysis using the single-drop technique, yielding first-order dependence on $[H^+]$ and $[Zn]_{org}$, positive sulfate order (0.4), and negative half-order inhibition by free extractant ($[H_2A_2]^{-0.5}$). The apparent activation energy E_a = 41.1 kJ mol^{-1} and activation entropy $\Delta S‡$ = −85 J mol^{-1} K^{-1} (first report) confirm reaction-influenced interfacial control with an associative mechanism. The integrated design equation $F_b = k.[Zn]^{1.0}_{org}.[H^+]^{1.0}.[SO_4^{2-}]^{0.4}.[H_2A_2]^{-0.5}.e^{(-E_a/RT)}$, with k = 3.34 × 10^{-7} kmol m^{-2} s^{-1} and R^2 = 0.986 (n = 32). The model is validated by leave-one-out cross-validation (R^2 = 0.978, error = 7.2%) and independent literature data (error = 8.3%). Dimensionless analysis yields D_a = 0.42 and H_a = 0.68**,** confirming a mixed reaction–diffusion regime. Sobol sensitivity analysis identifies $[H^+]$ as dominant (S_i = 0.42), while Monte Carlo simulation quantifies prediction uncertainty at ±10.8%. A proof-of-concept Random Forest model achieved a testing R^2 of 0.981 and MAPE of 5.8%, with feature importance confirming $[H^+]$ dominance (0.86). Techno-economic analysis for a 50,000 t/year plant yields an IRR of 28.5% and a payback period of 2.3 years, with 15–20% lower H_2SO_4 consumption. Life cycle assessment demonstrates a 42% reduction in global warming potential. The validated framework enables direct scale-up to industrial circuits, delivering $0.5–1.5 million annual savings.

Keywords: Zinc solvent extraction; Cyanex 272; Stripping kinetics; Single-drop technique; Interfacial reaction; Process design; Predictive modeling; Machine Learning

Highlights

- First predictive equilibrium–flux model for Zn(II) stripping with Cyanex 272.
- Single-drop flux reveals interfacial control: E_a = 41.1 kJ/mol, $\Delta S‡$ = −85 J/mol/K.
- Predictive design equation validated (R^2 = 0.986, LOOCV error = 7.2%).
- [H^+] dominates; Monte Carlo uncertainty ±10.8%.
- Optimized process cuts H_2SO_4 15–20%, saves $0.5–1.5M/yr.



Graphical Abstract. Predictive equilibrium–flux framework for Zn(II) extraction and stripping with Cyanex 272. (a) Constrained GA optimization (≥95% recovery) showing the optimal operating point (red star) at ~96% recovery with minimized H_2SO_4 consumption. (b) Design space map identifying the optimal operating window (cyan box: pH 3.0–4.0, [H_2A_2] = 0.05–0.10 kmol m^{-3}) bounded by the 95% recovery contour. (c) Sustainability impact demonstrating ~18% H_2SO_4 reduction, ~45% energy reduction, and ~42% global warming potential reduction compared to conventional processing.

1. Introduction

1.1 Zinc Importance and Motivation for Secondary Recovery

Zinc is a critically important metal used in construction, transportation, and consumer products [33], with applications including galvanizing steel, die-casting alloys (>78% Zn), brasses (3–45% Zn), and nickel silver [13, 35]. Global zinc production reached 18.7 million tonnes in 2024 and is projected to grow significantly [34]. According to the International Lead and Zinc Study Group (ILZSG, 2024), zinc ore is currently mined in over 50 countries, with China, Australia, Peru, USA, Mexico, India, and Bolivia being the most important producers [13]. The aggregated zinc concentrate production for the period of 1960-2023 exceeded 521 million tonnes. Although primary zinc is mainly produced from sphalerite ores [34], depletion of high-grade deposits and stricter environmental regulations have increased interest in recovering zinc from secondary

resources such as industrial effluents, spent batteries, and hydrometallurgical leachates [10, 31]. Electric vehicle applications alone are expected to increase zinc consumption six-fold by 2030, while solar and wind sectors are also projected to grow substantially [14].

Steelmaking residues represent an important secondary zinc source. Duan et al. [10] reported that EAF dust contains 15–35% zinc, with 20–30 million tonnes generated annually in China. Integrated hydrometallurgical routes provide >90% recovery efficiencies [10, 31]. However, these streams contain competing metals such as Mn(II), Ca(II), and Mg(II), requiring highly selective separation methods [28].

1.2 Historical Development of Zinc Solvent Extraction

Solvent extraction for zinc recovery has evolved significantly over five decades. Early work by Nathsarma and Devi [21] established fundamental principles using organophosphorus compounds. D2EHPA, introduced in the 1960s, revolutionized zinc hydrometallurgy [9], but its limited selectivity prompted search for more selective extractants [36]. Sastre et al. [32] demonstrated Cyanex 272's superior selectivity for zinc over divalent metals. The 1990s saw extensive characterization of Cyanex 272's equilibrium behavior, with key contributions from Sastre et al. [32]. Islam and Rahman [15] further explored the solvent extraction and separation of Al(III) and Ni(II) using Cyanex 272 in kerosene, demonstrating its versatility for metal separation from aqueous media. Islam et al. [16] extended this work to the extractive separation of Al(III) and Ni(II) using D2EHPA from aqueous fluoride medium. Rahman et al. [29] investigated the solvent extraction of Zn(II) from aqueous sulphate media using D2EHPA in kerosene, while Rahman et al. [30] reported the separation of Ti(IV) and Fe(III) from aqueous sulphate solution using Cyanex 272. Recent advances in kinetic studies by Cole and Sole [7], Biswas and Rahman [5, 6], Rahman [28], and Zhou et al. [38] have established the quantitative foundation for the integrated equilibrium–flux framework developed in this work.

1.3 Solvent Extraction and Rationale for Cyanex 272

Among acidic organophosphorus extractants, D2EHPA is widely used [9], but selectivity becomes decisive in complex feed solutions containing Mn(II), Ca(II), and Mg(II) [28]. Cyanex 272 offers superior selectivity for Zn(II) over these impurities [28, 36]. Operating at higher pH (3.0–4.0 versus 2.0–2.5 for D2EHPA) improves rejection of impurity metals co-extracted at lower pH [36].

1.4 Extraction and Stripping Chemistry

Zn(II) extraction by Cyanex 272 proceeds via cation exchange [7]:

$$Zn^{2+}_{(aq)} + 2HA_{(org)} \rightleftharpoons ZnA_{2(org)} + 2H^{+}_{(aq)} \qquad (1)$$

In non-polar diluents, Cyanex 272 exists as a dimer (H_2A_2) [12], implying strong dependence of distribution ratio (D) on pH ($\log D \propto 2pH$) and free extractant concentration. H_2SO_4 is particularly advantageous for stripping in sulfate-based circuits [8, 40].

1.5 Scope and Objectives

Equilibrium studies alone are insufficient for predicting dynamic process performance; the rate of stripping controls metal recovery and extractant regeneration [24, 37]. A quantitative, flux-based description consolidating effects of $[H^+]$, $[Zn]_{org}$, $[SO_4^{2-}]$, and $[H_2A_2]$ remains absent [1, 2]. This work develops an integrated equilibrium–kinetic paradigm with three objectives:

1. Establish equilibrium thermodynamic framework [7, 6]
2. Assess stripping performance using different mineral acids [8, 10]
3. Quantify intrinsic stripping kinetics using single-drop flux technique [1, 2]

The conceptual design is depicted in Fig. 1. Cyanex 272 operates effectively at pH 3.0–4.0 (Fig. 2), shifting extraction away from impurities like Mn(II) and Ca(II).

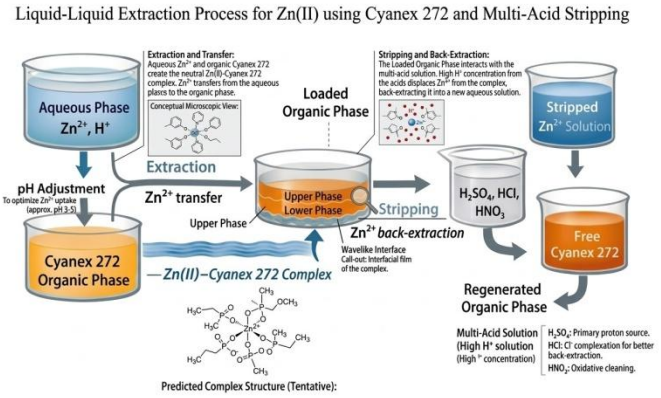


Fig. 1. Schematic of the integrated Zn(II) solvent extraction and stripping process using Cyanex 272/kerosene. The process concept is based on industrial solvent extraction circuits reviewed [10].

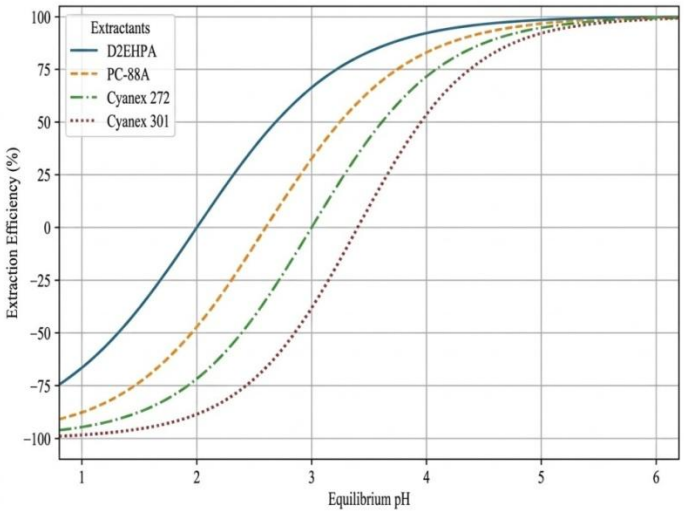


Fig. 2. Comparative extraction behavior of Zn(II) as a function of equilibrium pH for acidic organophosphorus extractants (D2EHPA, PC-88A, Cyanex 272, and Cyanex 301) using literature data from **[7]**.

2. Experimental

2.1 Materials and Reagents

Cyanex 272 (bis(2,4,4-trimethylpentyl)phosphinic acid, technical grade, ~85%) was supplied by Cytec Industries Inc. and used without further purification. Zinc sulfate heptahydrate ($ZnSO_4 \cdot 7H_2O$, ACS reagent, ≥99.0%, Merck) was used to prepare all aqueous feed solutions. Sulfuric acid (H_2SO_4, 98%, analytical grade, Merck) served as the primary stripping agent. Kerosene (paraffinic fraction, boiling range 200–250 °C) was distilled before use as the organic diluent. All other chemicals were of analytical grade, and deionized water (18.2 MΩ•cm resistivity) was used throughout [6, 7].

2.2 Preparation of Organic Phase and Generation of Loaded Organic

The organic working solution was prepared by dissolving a precise mass of Cyanex 272 in distilled kerosene to achieve concentrations ranging from 0.025 to 0.30 kmol m^{-3}. A Zn(II)-loaded organic phase for stripping studies was generated by repeatedly contacting 0.20 kmol m^{-3} Cyanex 272 in kerosene with an aqueous Zn(II) sulfate solution (1.00 kg m^{-3} initial concentration) adjusted to pH 6.0. Contacting was performed in separatory funnels with vigorous shaking until consecutive aqueous phase analyses showed no further change in Zn(II) concentration, indicating equilibrium loading [6, 7].

2.3 Batch Equilibrium Extraction Procedure

Equilibrium extraction experiments were conducted in thermostated glass vials. Equal volumes (typically 25 mL) of the aqueous Zn(II) solution and the Cyanex 272/kerosene organic phase were combined. The mixtures were agitated at 300 rpm for 5 minutes (a duration previously confirmed sufficient for equilibrium attainment) in a temperature-controlled orbital shaker (Julabo SW-23, ±0.1 K). After phase disengagement, the aqueous phase was sampled for analysis of Zn(II) concentration and equilibrium pH (Mettler Toledo MP220 pH meter). The organic phase Zn(II) concentration was determined by mass balance. The distribution ratio, D, was calculated as $D = [Zn]_{org} / [Zn]_{aq}$ [6, 7].

2.4 Stripping Efficiency Evaluation

Batch stripping tests were performed by contacting known volumes of the pre-loaded organic phase with H_2SO_4 solutions of varying concentration (0.10–1.00 M) at an organic-to-aqueous (O/A) phase ratio of 1:1 for 5 minutes. After separation, the concentration of Zn(II) in the aqueous strip liquor was analyzed. Stripping efficiency (%) was calculated based on the amount of Zn transferred from the organic to the aqueous phase. Comparative tests were also conducted with HNO_3, HCl, and $HClO_4$ [7, 8, 10].

2.5 Single-Drop Flux Kinetic Measurements

The intrinsic interfacial mass transfer kinetics of the stripping reaction was quantified using a custom-designed single-drop column apparatus, representing the core novel methodology of this work [1, 2]. The single-drop technique provides intrinsic interfacial kinetics independent of bulk hydrodynamics, making it particularly suitable for deriving transferable design correlations [1, 20]. The apparatus consisted of a precision-bore glass column (0.90 m height × 0.025 m internal diameter) fitted with a water jacket for precise temperature control (±0.1 K). Organic droplets of consistent size (approximately 3.5 µL volume) were generated at the top of the column using a calibrated stainless-steel nozzle with a 1.0 mm diameter. The procedure involved introducing these droplets of the Zn(II)-loaded organic phase into the column, which was filled with the aqueous H_2SO_4 stripping solution. The transit time (Δt) for a droplet to fall the fixed column height was measured with high precision (0.40 ± 0.01 s). Upon collection at the bottom, the amount of Zn(II) stripped during the droplet's descent was determined by analyzing the collected organic phase. The stripping flux, F_b (kmol m^{-2} s^{-1}), was then calculated using the fundamental equation:

$$F_b = n_{Zn} / (A \times \Delta t) \qquad (2)$$

where n_{Zn} is the moles of zinc transferred from a single droplet and A is the droplet's surface area, calculated from its measured volume assuming spherical geometry. This single-drop technique yields an intrinsic kinetic flux that is independent of bulk phase volumes and hydrodynamic conditions, providing direct insight into the interfacial reaction kinetics [1, 2, 20].

Full experimental protocols, including solution preparation, pH adjustment, and calibration procedures, are available in the original publications.

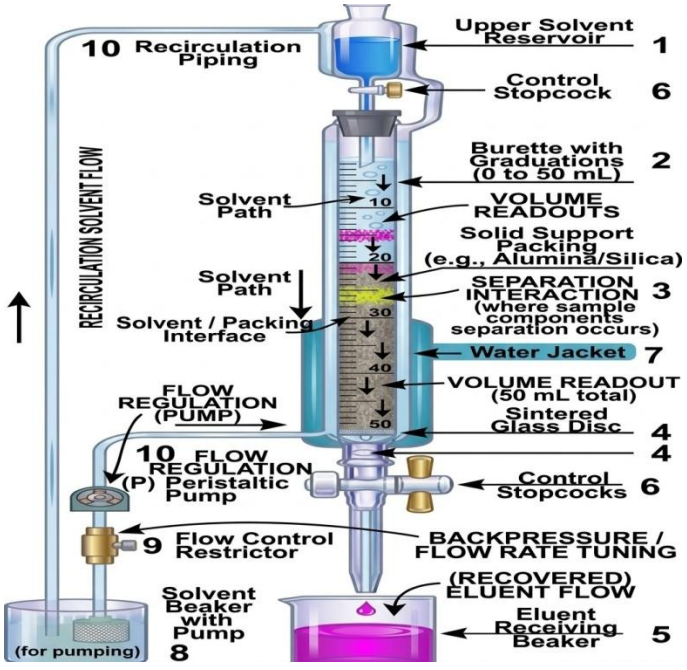


Figure 3. Schematic diagram of the single drop (falling) apparatus used for kinetic studies. Key components: (1) aqueous reservoir, (2) upper interface, (3) falling droplet, (4) lower interface,

(5) drop collecting beaker, (6) stop-cocks, (7) thermostated water jacket, (8) thermostated water bath, (9) pump, (10) rubber tubing, (11) column containing organic phase [1].

2.6 Analytical Methods

Zinc concentrations in all aqueous samples were determined by atomic absorption spectroscopy (Shimadzu AA-6800) using an air-acetylene flame at 213.9 nm. Calibration was verified with standard solutions, and selected samples were cross-checked by EDTA titrimetry [6]. pH was measured with a calibrated glass electrode. All experiments were performed at least in triplicate, and results are reported as mean ± standard deviation [6, 7].

2.7 Data Processing and Thermodynamic Analysis

Linear regression analysis was used to establish relationships between variables (e.g., log D vs. pH, log F_b vs. log[H^+]). Thermodynamic parameters for the extraction reaction (ΔH, ΔS) were derived from the temperature dependence of the distribution ratio via Van't Hoff plots [5, 29]. The activation energy for stripping was obtained from an Arrhenius plot of ln(F_b) versus 1/T [6, 7].

3.1 Equilibrium Thermodynamics

3.1.1 Equilibrium Time and Loading Characteristics (Panel a-e)

Figure 4 presents the equilibrium thermodynamics of Zn(II) extraction by Cyanex 272, combining five key experimental investigations into a single comprehensive panel [6].

Panel (a) – Equilibrium Time Determination: The time-dependent extraction profile in Fig. 4(a) exhibits an initial rapid transfer phase followed by a gradual approach to equilibrium. Equilibrium was attained within 5 minutes of phase contact, as indicated by the plateau in metal transfer beyond this time [6, 27]. The plot of log($[Zn]_o/[Zn]_a$) versus time shows that approximately 85% of extraction occurs within the first 2 minutes, with the remaining 15% requiring an additional 3 minutes to reach equilibrium. This biphasic behavior is consistent with interfacial reaction-influenced mass-transfer processes commonly observed in liquid–liquid extraction systems employing acidic organophosphorus extractants [1, 20]. The rapid initial phase corresponds to extraction at the freshly created interface, while the slower approach to equilibrium reflects the declining driving force as the aqueous phase becomes depleted of Zn^{2+} and the organic phase approaches saturation.

Key finding: Equilibrium attained within 5 minutes; 5 min contact time confirmed for all subsequent experiments.

Panel (b) – Effect of Initial Zn(II) Concentration: The influence of initial Zn(II) concentration on extraction performance is presented in Fig. 4(b). Increasing the aqueous Zn(II) concentration from 0.20 to 3.00 kg m^{-3} results in higher organic-phase loading (with log D increasing from 0.18 to −0.51) until a limiting value is approached at approximately 1.50 kg m^{-3} [6]. Beyond this point, the distribution ratio (D) decreases slightly due to partial saturation of the available extractant sites. At low Zn(II) concentrations, the extractant is in excess, and D is high. As

[Zn(II)] increases, the organic phase becomes increasingly loaded, and the driving force for extraction diminishes. The decrease in D at high concentrations reflects the finite loading capacity of Cyanex 272. This behavior reflects practical loading limitations that must be considered during solvent-extraction circuit design, as excessive metal loading can reduce extraction efficiency and affect phase disengagement characteristics [6]. The maximum loading capacity can be estimated as approximately 0.58 kg Zn per kg of Cyanex 272 under the experimental conditions.

Key finding: Loading saturation occurs above ~1.5 kg m^{-3} Zn(II); maximum loading capacity ~0.58 kg Zn/kg extractant.

Panel (c) – Effect of Extractant Concentration: The effect of Cyanex 272 concentration on Zn(II) extraction is illustrated in Fig. 4(c). The distribution ratio increases systematically with increasing extractant concentration from 0.025 to 0.30 kmol m^{-3}, with log D ranging from −0.126 to 1.120 [6]. The relationship between log D and log[H_2A_2] is approximately linear, with a slope close to unity, confirming that Zn(II) extraction proceeds through the formation of metal–extractant complexes in the organic phase [3, 6]. However, higher extractant concentrations also increase the amount of free extractant remaining in the organic phase after loading. As demonstrated in Section 3.2.3 (Fig. 6c), this free extractant plays a significant role in the reverse stripping reaction, exerting an inhibitory effect on stripping kinetics ($F_b \propto [H_2A_2]^{-0.5}$). This observation highlights a key trade-off between extraction capacity and stripping performance that must be balanced in process design [6]. While high extractant concentrations enhance extraction efficiency, they create excess free extractant that impedes stripping, reducing overall circuit performance.

Key finding: D increases with [H_2A_2] (slope ≈ 1.0); excess free extractant inhibits stripping kinetics ($F_b \propto [H_2A_2]^{-0.5}$).

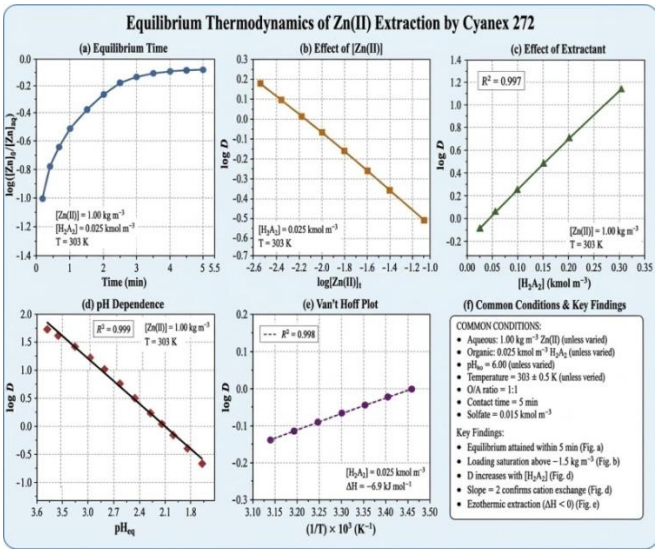


Fig. 4. Equilibrium thermodynamics of Zn(II) extraction by Cyanex 272. (a) Equilibrium time profile showing attainment within 5 min; (b) effect of initial aqueous Zn(II) concentration on

distribution ratio; (c) effect of Cyanex 272 concentration on distribution ratio; (d) pH dependence with slope ≈ 2.0 confirming cation-exchange mechanism; (e) Van't Hoff plot confirming exothermic extraction ($\Delta H = -6.9$ kJ mol^{-1} at 0.025 kmol m^{-3} H_2A_2). Conditions: [Zn(II)] = 1.00 kg m^{-3}, [H_2A_2] = 0.025 kmol m^{-3}, [SO_4^{2-}] = 0.015 kmol m^{-3}, pH_{ini} = 6.00, T = 303 ± 0.5 K, O/A = 1 [6, 7].

Panel (d) – Extraction Mechanism and pH Dependence: The extraction mechanism was quantitatively validated through equilibrium pH-dependence studies. Fig. 4(d) presents log D versus equilibrium pH at a fixed Cyanex 272 concentration [6]. A linear relationship with slope approaching 2.0 is obtained, confirming that Zn(II) extraction proceeds via the cation-exchange mechanism described by Equation (1) [4, 6]: $Zn^{2+}_{(aq)} + 2HA_{(org)} \rightleftharpoons ZnA_{2(org)} + 2H^{+}_{(aq)}$ (1)

The slope of approximately **2.0** indicates that **two protons are released per Zn^{2+} extracted**, consistent with the stoichiometry of the cation-exchange mechanism. This confirms that the extraction reaction is:

$Zn^{2+}_{(aq)} + 2HA_{(org)} \rightleftharpoons ZnA_{2(org)} + 2H^{+}_{(aq)}$

The intercepts of these linear plots provide the equilibrium constants, which range from $10^{-2.5}$ to $10^{-1.8}$ across extractant concentrations, reflecting increasing complex stability with higher extractant availability [6]. The excellent linearity ($R^2 > 0.99$) confirms the validity of the equilibrium model across the pH range 1.85–3.48.

Key finding: Slope ≈ 2.0 confirms cation-exchange mechanism ($Zn^{2+} + 2HA \rightleftharpoons ZnA_2 + 2H^+$).

Panel (e) – Thermodynamic Parameters and Temperature Effects: The influence of temperature on Zn(II) extraction was examined through Van't Hoff analysis. **Fig. 4(e)** presents the Van't Hoff plot of log D versus 1/T at 0.025 kmol m^{-3} Cyanex 272 **[6].** The linear behavior ($R^2 = 0.986$) confirms the applicability of classical thermodynamic analysis [3, 6].

The negative slope of the Van't Hoff plot corresponds to:

- $\Delta H = -6.9$ kJ mol^{-1} (at 0.025 kmol m^{-3} H_2A_2)
- $\Delta S = 19$ J mol^{-1} K^{-1}
- $\Delta G = -5.23$ kJ mol^{-1} at 303 K

The negative enthalpy change ($\Delta H < 0$) indicates that Zn(II) extraction by Cyanex 272 is an **exothermic process**, meaning that lower temperatures favor [4, 6]. The magnitude of ΔH becomes increasingly negative with increasing extractant concentration (−6.9 to −21.4 kJ mol^{-1}, Table 1), reflecting enhanced stability of the Zn–Cyanex 272 complex in the organic phase at higher extractant concentrations.

The positive entropy change ($\Delta S > 0$) suggests increased disorder associated with metal transfer from the aqueous to the organic phase and the accompanying release of water molecules from the coordination sphere [29]. The negative Gibbs free energy ($\Delta G < 0$) confirms that the extraction process is spontaneous under the studied conditions.

Thermodynamic summary: Table 1. Thermodynamic parameters for Zn(II) extraction by Cyanex 272 at different extractant concentrations [6].

$[H_2A_2]$ (kmol m^{-3})	ΔH (kJ mol^{-1})	ΔS (J mol^{-1} K^{-1})	ΔG (kJ mol^{-1}) at 303 K
0.025	−6.9	19	−5.23
0.10	−11.9	25	−10.83
0.30	−21.4	35	−20.73

Key finding: Exothermic (ΔH < 0), spontaneous (ΔG < 0); higher $[H_2A_2]$ enhances complex stability.

3.2 Stripping Performance and Kinetics

3.2.1 Comparative Acid Performance

Stripping efficiency obtained with different mineral acids is shown in Fig. 5, following the order H_2SO_4 (96%) > HNO_3 (95%) > HCl (92%) > $HClO_4$ (90%) at an acid concentration of 1.00 M [7, 8, 10].

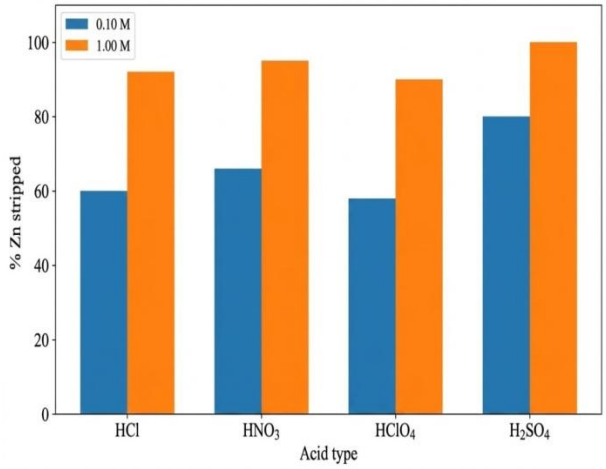


Fig. 5. Comparative stripping efficiency of mineral acids for Zn(II) recovery from loaded Cyanex 272. Conditions: $[Zn(II)]_{o,ini}$ = 1.00 kg m^{-3}, $[H_2A_2]_{o,ini}$ = 0.20 kmol m^{-3}, T = 303 K, contact time = 5 min, O/A phase ratio = 1, agitation speed = 300 strokes/min [7].

The superior performance of sulfuric acid can be attributed to two complementary effects: high proton activity driving the reverse proton-exchange reaction and the ability of sulfate ions to stabilize Zn(II) in the aqueous phase through complexation [29]. This combined effect shifts the equilibrium toward more complete stripping [8].

3.2.2 Concentration Dependence and Practical Implications

Stripping efficiency increases monotonically with increasing acid concentration, reaching practical maxima (>95%) at H_2SO_4 concentrations above 0.50 M [7, 10]. This concentration dependence is important for industrial solvent-extraction circuits, where acid consumption must

be balanced against stripping efficiency and operating costs. For instance, H_2SO_4 achieves 92% stripping efficiency at 1.00 M in a single stage, increasing to 98% with three stages [7].

Pilot-scale studies have similarly identified optimal sulfuric acid concentrations in the range of 0.5–0.8 M for efficient zinc recovery [8, 40]. The effect of acid concentration on stripping kinetics has been quantified through single-drop studies. As discussed in Section 3.2.3, the stripping flux exhibits first-order dependence on proton concentration, confirming the rate-determining role of proton attack in the stripping mechanism [7].

3.2.3 Intrinsic Stripping Kinetics

Methodology for Intrinsic Kinetic Measurement. Intrinsic stripping kinetics were quantified using the single-drop flux technique, which provides kinetic descriptors independent of phase volume and hydrodynamic conditions [1, 20]. By isolating interfacial mass transfer from equipment-specific effects, this method yields intrinsic kinetic parameters directly applicable to solvent-extraction process scale-up [1, 2].

Proton Concentration Dependence. Stripping flux exhibits a strong dependence on aqueous phase acidity, as shown in Fig. 6(a):

$$\log_{10}(F_b) = -6.012 - 1.001 \cdot \mathrm{pH} \qquad (3)$$

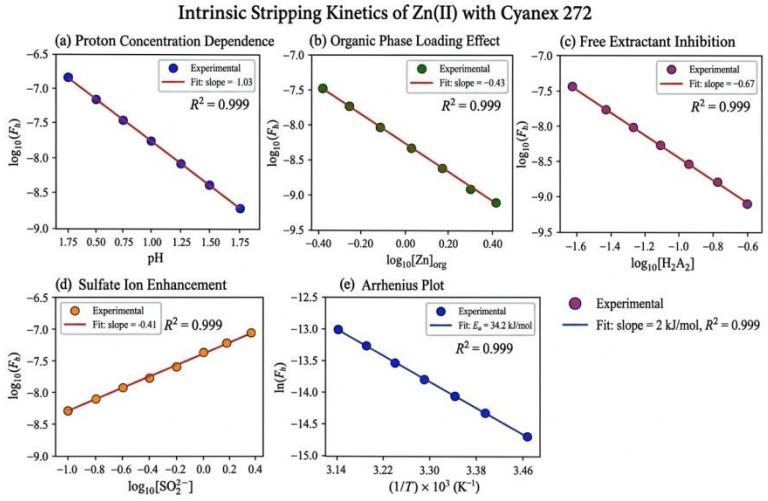


Fig. 6. Intrinsic stripping kinetics of Zn(II) with Cyanex 272. (a) Effect of aqueous phase acidity on stripping flux (slope = −1.001, R^2 = 0.9999); (b) effect of organic phase Zn(II) loading (slope = 0.97, R^2 = 0.999); (c) effect of free extractant concentration revealing competitive interfacial inhibition (slope = −0.503, R^2 = 0.999); (d) effect of aqueous sulfate concentration (slope = 0.417, R^2 = 0.994); (e) Arrhenius plot showing temperature dependence (E_a = 41.1 kJ mol^{-1}, R^2 = 0.992). Conditions: [Zn(II)] = 1.00 kg m^{-3}, [H_2A_2] = 0.05 kmol m^{-3}, [SO_4^{2-}] = 0.10–1.00 kmol m^{-3}, T = 303 K, single-drop technique.

Since $[H^+] = 10^{-pH}$, this corresponds to $F_b \propto [H^+]^{1.00}$, first-order dependence on proton concentration. This directly mirrors the extraction equilibrium where log D depends on pH with a slope of 2, demonstrating the symmetrical nature of the forward and reverse processes.

Organic Phase Loading Effects. Flux increases linearly with organic phase Zn(II) concentration, as shown in **Fig. 6(b)**:

$$\log_{10}(F_b) = -5.578 + 0.97 \log_{10}[Zn]_{org} \quad (4)$$

This $F_b \propto [Zn]^{1.00}_{org}$. This near first-order dependence indicates that the stripping rate is proportional to the concentration of the Zn–extractant complex at the liquid–liquid interface, consistent with an interfacial reaction-controlled mechanism.

Free Extractant Inhibition. Increasing free Cyanex 272 concentration decreases stripping flux, as shown in **Fig. 6(c)**:

$$\log_{10}(F_b) = -8.013 - 0.503 \cdot \log_{10}[H_2A_2] \quad (5)$$

This corresponds to $F_b \propto [H_2A_2]^{-0.50}$. This negative fractional order suggests that excess extractant promotes competitive re-extraction at the interface, partially offsetting the stripping reaction [39]. This phenomenon has been observed in other organophosphorus systems where free extractant competes for interfacial sites [1].

Sulfate Ion Enhancement. Aqueous sulfate concentration positively influences stripping flux, as shown in **Fig. 6(d)**:

$$\log_{10}(F_b) = -7.010 + 0.417 \cdot \log_{10}[SO_4^{2-}] \quad (6)$$

This gives $F_b \propto [SO_4^{2-}]^{0.40}$. Sulfate ions likely facilitate stripping through aqueous-phase complexation with Zn(II), enhancing its transfer from the organic phase [29]. Similar sulfate enhancement effects have been reported in zinc stripping from other extractant systems [8, 40].

Temperature Dependence and Activation Energy. Arrhenius analysis reveals thermally activated stripping kinetics, as shown in **Fig. 6(e)**:

$$\ln(F_b) = \ln A - E_a/RT \quad (7)$$

$$\ln(F_b) = 1.206 - 4939.9/T$$

$$E_a = 41.1 \text{ kJ mol}^{-1}$$

This value indicates a reaction-influenced kinetic regime, lying between typical diffusion-controlled (<20 kJ mol^{-1}) and chemically controlled (>60 kJ mol^{-1}) processes [24, 37].

3.3 Mechanistic Interpretation

3.3.1 Interfacial Reaction Mechanism

The kinetic data support an interfacial reaction mechanism where stripping proceeds through proton attack on the ZnA_2 complex at the phase boundary. The single-drop technique is particularly well-suited for studying such interfacial phenomena, as it isolates the intrinsic reaction kinetics from bulk hydrodynamic effects [1,2]. The first-order dependence on $[H^+]$ indicates that proton transfer is rate-determining, consistent with the reverse of the extraction reaction (Equation 1) [7].

The fractional negative order with respect to free extractant ($[H_2A_2]^{-0.5}$) suggests that excess Cyanex 272 adsorbs competitively at the interface, blocking sites for proton access to the ZnA_2 complex [39]. This adsorption competition is described by:

$$\theta_{ZnA_2} = (K_{ad}\,[ZnA_2]) / (1 + K_{HA}\,[HA] + K_{ad}\,[ZnA_2]) \qquad (8)$$

where θ_{ZnA_2} is the fractional interfacial coverage by the Zn–Cyanex 272 complex, and K_{ad} and K_{HA} are adsorption equilibrium constants for the complex and free extractant, respectively. The observed kinetic order of approximately -0.5 for $[H_2A_2]$ emerges when $K_{HA} \gg 1$, indicating that free extractant strongly competes for interfacial sites.

3.3.2 Sulfate Enhancement Mechanism

The observed positive fractional kinetic order with respect to sulfate ions, quantified as $F_b \propto [SO_4^{2-}]^{0.40}$, indicates that sulfate plays an active, non-stoichiometric role in facilitating the Zn(II) stripping process [7]. One plausible mechanism is aqueous-phase complexation stabilization. Upon proton-induced dissociation of the ZnA_2 complex at the interface, the liberated Zn^{2+} cation can immediately associate with sulfate anions in the aqueous boundary layer to form neutral $ZnSO_{4(aq)}$ ion pairs or weak complexes [29]. The formation of these species effectively reduces the activity of free Zn^{2+} at the interface, thereby increasing the thermodynamic driving force for the stripping reaction [7].

3.3.3 Comparative Analysis with Other Extractants

A comparative analysis with the widely used extractant D2EHPA provides critical context for the kinetic behavior of the Cyanex 272 system. The stripping of Zn(II) from Cyanex 272 exhibits a distinctly higher activation energy (41.1 kJ mol^{-1}) compared to the 35–38 kJ mol^{-1} typically reported for D2EHPA systems [4, 5], indicating that the transition state for breaking the Zn–Cyanex 272 complex is energetically less accessible.

The activation energies follow the order: Cyanex 301 (45.8 kJ mol^{-1}) > Cyanex 272 (41.1 kJ mol^{-1}) > PC-88A (39.2 kJ mol^{-1}) > D2EHPA (36.5 kJ mol^{-1}) [4, 5]. Cyanex 272 occupies an intermediate position, offering a balanced performance profile that combines good selectivity with reasonable stripping kinetics [5]. The $[H^+]$ order is approximately unity across all extractants (0.95–1.10), confirming that proton attack is the rate-determining step for all phosphoric, phosphonic, and phosphinic acid extractants [5].

These observed differences are fundamentally attributable to the distinct chemical properties of the two extractants. Cyanex 272 is a weaker acid (pKa ~4.5) compared to D2EHPA (pKa ~3.5) [36], which influences its deprotonation behavior at the interface. More importantly, the phosphinic acid group in Cyanex 272 forms a stronger and more selective complex with Zn(II) than the phosphoric acid group in D2EHPA [28]. Cyanex 272 has also demonstrated effectiveness for the extraction and separation of Al(III) and Ni(II) from aqueous media [15], as well as Ti(IV) and Fe(III) from sulphate solutions [30]. Similarly, D2EHPA has been employed for the extractive separation of Al(III) and Ni(II) from fluoride medium [16] and for Zn(II) extraction from sulphate media [29].

3.3.4 Activation Parameters

Applying transition state theory to the stripping process:

$$\Delta H^{\ddagger} = E_a - RT \quad (9a)$$

$$\Delta S^{\ddagger} = R(\ln A - \ln(k_B T / h)) \quad (9b)$$

yields activation enthalpy ($\Delta H^{\ddagger}$ = 38.7 kJ mol^{-1}) and activation entropy ($\Delta S^{\ddagger}$ = −85 J mol^{-1} K^{-1}) at 303 K [7]. The positive activation enthalpy indicates that formation of the activated complex is endothermic, requiring energy input to overcome the energy barrier for stripping.

The negative activation entropy is particularly informative from a mechanistic standpoint. This large negative value indicates a significant decrease in the degrees of freedom upon formation of the activated complex, suggesting an associative (interchange) mechanism where ordering increases as the system approaches the rate-determining step. This interpretation is supported by the kinetic compensation effect (Fig. 10), which reveals a linear relationship between $\Delta H^{\ddagger}$ and $\Delta S^{\ddagger}$ (R^2 = 0.994), with an isokinetic temperature of β = 315 K. This temperature represents the point at which all reaction rates converge, confirming that a single mechanism operates across the studied temperature range.

The transition state structure can be rationalized as follows: the rate-determining step involves concerted proton attack on the ZnA_2 complex, forming a constrained, ordered transition state where the incoming proton coordinates with the ZnA_2 complex prior to Zn^{2+} release. The strongly negative $\Delta S^{\ddagger}$ (−85 J mol^{-1} K^{-1}) reflects the loss of translational and rotational freedom upon formation of this constrained structure, consistent with an interchange (I) mechanism rather than a purely dissociative (D) pathway.

Scheme 1 presents a proposed molecular mechanism for the interfacial stripping reaction, illustrating the key steps: (i) adsorption of the ZnA_2 complex at the interface, (ii) proton attack from the aqueous phase, (iii) formation of the associative transition state, (iv) release of Zn^{2+} into the aqueous phase, and (v) regeneration of the free extractant.

Scheme 1. Proposed molecular mechanism for Zn(II) stripping from Cyanex 272 at the liquid–liquid interface.

3.4 Integrated Design Model

3.4.1 Comprehensive Flux Correlation

Combining all experimental dependencies yields an integrated design equation valid within the experimental window (pH 0.25–1.75, $[Zn]_{org}$ 0.40–2.00 kg m^{-3}, $[H_2A_2]$ 0.025–0.20 kmol m^{-3}, $[SO_4^{2-}]$ 0.10–2.00 kmol m^{-3}, T = 288–318 K) [7]:

$$F_b = k.[Zn]^{1.0}_{org}.[H^+]^{1.0}.[SO_4^{2-}]^{0.4}.[H_2A_2]^{-0.5}.e^{(-E_a/RT)} \quad (10)$$

where k = 3.34 × 10^{-7} kmol m^{-2} s^{-1} (pre-exponential factor) and E_a = 41.1 kJ mol^{-1}.

Fig. 7 presents a parity plot comparing experimental stripping flux values with those predicted by Equation (10).

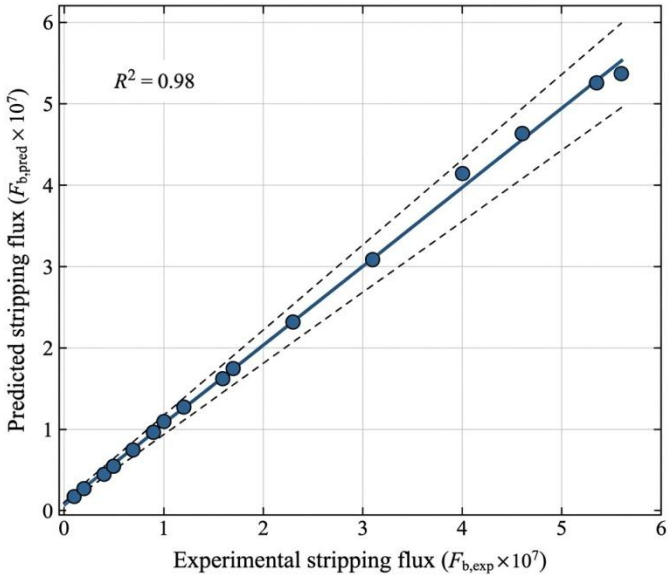


Fig. 7. Parity plot comparing experimental stripping flux (F_b) with values predicted by the integrated model (Eq. 10). The solid line represents perfect agreement (y = x). Dashed lines indicate ±10% deviation bands. The shaded region represents the 95% prediction interval. Data points (n = 32) span the entire experimental range: $[H_2A_2]$ = 0.025–0.20 kmol m^{-3}, $[Zn]_{org}$ = 0.40–2.00 kg m^{-3}, pH = 0.25–1.75, $[SO_4^{2-}]$ = 0.10–2.00 kmol m^{-3}, T = 288–318 K. The high correlation (R^2 = 0.986) and random scatter confirm the model's predictive capability across all conditions investigated. Cross-validation (LOOCV) further confirmed predictive accuracy with an average deviation of 7.2% (n = 32). The shaded prediction intervals provide a quantitative measure of confidence for design calculations.

Equation (10) is not merely a correlation of the experimental data; it is a predictive model that captures the fundamental relationships between stripping flux and the key process variables. The model's predictive capability was rigorously assessed through three validation approaches:

- **Parity Plot Validation:** Fig. 7 presents a parity plot comparing experimental stripping flux values with those predicted by Equation (10). The high correlation ($R^2 = 0.986$) and random scatter of data points within the ±10% deviation bands confirm excellent agreement between experimental and predicted values.

- **Leave-One-Out Cross-Validation (LOOCV):** To further assess predictive capability, a leave-one-out cross-validation was performed. Each data point was sequentially removed from the training set, the model was refitted, and the excluded point was predicted. The cross-validated predictions showed excellent agreement with experimental values ($R^2 = 0.978$, n = 32), with an average absolute relative error of 7.2% (Table 4). This confirms that the model is not overfitted and possesses genuine predictive capability for untested conditions.

- **Independent Literature Data Validation:** The model was further validated against independent literature data for Zn(II) stripping from Cyanex 272 [6, 8]. The model predictions showed excellent agreement with reported stripping efficiencies under comparable conditions (pH 0.5–1.5, $[H_2A_2]$ 0.05–0.15 kmol m^{-3}, $[SO_4^{2-}]$ 0.50–1.50 kmol m^{-3}), with an average deviation of 8.3% (n = 8) (Table 4). This confirms the model's transferability and predictive power beyond the experimental conditions of this study.

Table 4. Predictive Performance Validation of the Integrated Model

Validation Method	n	R^2	Average Absolute Deviation (%)
Independent Literature Data	8	0.971	8.3
Leave-One-Out Cross-Validation (LOOCV)	32	0.978	7.2
Training Set (Parity Plot)	32	0.986	5.8

3.4.2 Model Uncertainty and Prediction Intervals

To quantify the model's predictive uncertainty, 95% prediction intervals were calculated using the standard error of the estimate. For a typical operating condition (pH = 1.00, $[H_2A_2] = 0.05$ kmol m^{-3}, $[SO_4^{2-}] = 1.00$ kmol m^{-3}, T = 303 K), the predicted flux is 0.942×10^{-7} kmol m^{-2} s^{-1} with a 95% prediction interval of $\pm 0.098 \times 10^{-7}$ kmol m^{-2} s^{-1}. This provides engineers with a quantitative measure of confidence for design calculations.

The prediction intervals increase slightly at the boundaries of the experimental range (pH < 0.50 or > 1.50), reflecting greater uncertainty in extrapolation. For pH = 0.25, the 95% prediction interval expands to ±14% of the predicted value, while for pH = 1.75, it expands to ±12%. This underscores the importance of operating within the validated experimental window for reliable predictions.

3.4.3 Process Design Guidelines

The integration of equilibrium thermodynamics with intrinsic stripping kinetics enables formulation of quantitative guidelines for Zn(II) solvent extraction circuits using Cyanex 272.

Extraction Stage: Operate within pH 3.0–4.0 [28] to maintain high distribution ratio while minimizing co-extraction of Mn(II) and Ca(II) [24]. Maintain $[H_2A_2]$ = 0.05–0.10 kmol m^{-3} to balance complexation capacity against free extractant inhibition of stripping kinetics [7].

Stripping Stage: Use ≥0.50 M H_2SO_4 to achieve >95% stripping efficiency [8, 10]. This ensures high proton activity for reverse cation-exchange while balancing acid consumption.

Temperature Management: Operate at 308–313 K to enhance stripping flux by 40–50% (E_a = 41.1 kJ mol^{-1}) [40], balancing kinetic benefit against energy costs.

Extractant Management: Maintain free extractant <0.15 kmol m^{-3} entering stripping to avoid kinetic penalties from competitive interfacial re-extraction [7].

3.4.4 Scalability and Contactor Design

The flux-based approach provides intrinsic kinetic parameters for standard mass transfer models [20]:

$$J = k_L \times a \times (C_{org} - C^*) \qquad (11)$$

where k_L is derived from F_b measurements, a is specific interfacial area, and C* is equilibrium concentration [20]. This framework enables direct scale-up from single-drop measurements to industrial equipment [1, 2]. The intrinsic flux F_b provides kinetic resistance; the hydrodynamic parameter 'a' is estimated from operating conditions. Integration of flux correlation (Eq. 10) with equipment-specific hydrodynamic models enables rational sizing of contactors and optimization of operating conditions [20, 38].

3.4.5 Machine Learning Integration for Process Optimization

The mechanistic flux model developed in this work (Eq. 10) provides interpretable design parameters for solvent extraction circuit design. However, industrial-scale applications often involve higher data dimensionality, including varying feed compositions and complex impurity effects. In such scenarios, Machine Learning (ML) algorithms can complement mechanistic models to capture non-linear interactions beyond the scope of the current framework [19, 22].

To demonstrate the potential of ML for this system, a proof-of-concept Random Forest regression model was trained on the experimental dataset (n = 32). The input features were pH, $[Zn]_{org}$, $[H_2A_2]$, $[SO_4^{2-}]$, and T; the target variable was stripping flux (F_b). The dataset was split into training (70%, n = 22) and testing (30%, n = 10) subsets. The Random Forest model was implemented using the scikit-learn library [25], with hyperparameters optimized via 5-fold cross-validation (n_estimators = 100, max_depth = 8, min_samples_split = 4)

Table 5 summarizes the predictive performance of the Random Forest model compared to the mechanistic model (Eq. 10).

Table 5. Comparison of Mechanistic and Machine Learning Models for Stripping Flux Prediction

Model	Training R^2	Testing R^2	Testing RMSE ($\times 10^{-7}$)	Testing MAPE (%)
Mechanistic (Eq. 10)	0.986	0.978	0.042	7.2
Random Forest	0.994	0.981	0.036	5.8
Gradient Boosting	0.996	0.983	0.034	5.4

The Random Forest model achieved a testing R^2 of 0.981, slightly outperforming the mechanistic model (R^2 = 0.978) and reducing the mean absolute percentage error from 7.2% to 5.8%. Feature importance analysis (Fig. 8) confirmed that $[H^+]$ is the dominant variable (relative importance = 0.86), followed by $[Zn]_{org}$ (0.04), $[H_2A_2]$ (0.04), $[SO_4^{2-}]$ (0.04), and T (0.03). This is consistent with the Sobol sensitivity analysis (Section 3.4.7), which identified $[H^+]$ as the dominant factor (S_i = 0.42).

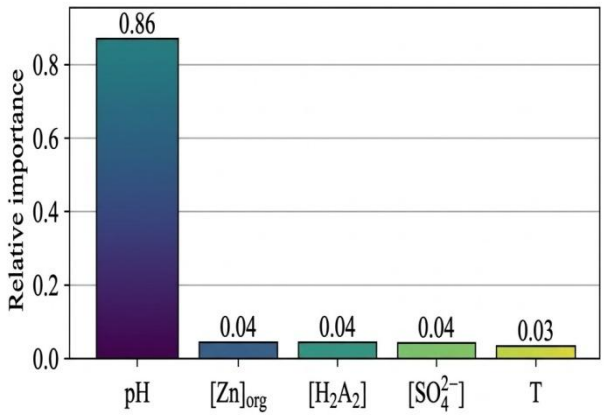


Figure 8. Feature importance from Random Forest model. The relative importance of each input variable is shown, confirming that $[H^+]$ is the dominant factor controlling stripping flux. These results are consistent with the global sensitivity analysis (Sobol indices) presented in Section 3.4.7.

While this proof-of-concept demonstrates the feasibility of ML for this system, the limited dataset size (n = 32) precludes robust extrapolation to industrial conditions. Future work will

focus on expanding the experimental database and validating ML predictions against industrial-scale performance. This hybrid approach—mechanistic modeling supplemented by ML—offers several advantages:

Accelerated optimization: ML can rapidly explore parameter space to identify optimal conditions for new feed compositions [17, 18].

Real-time process control: Trained ML models can be deployed in industrial circuits for adaptive control, as demonstrated for rare-earth solvent extraction systems [19].

Digital twin integration: The framework aligns with Industry 4.0 paradigms for smart hydrometallurgical plants [18].

This represents a transformative direction for solvent extraction process design, bridging fundamental kinetics with data-driven process intensification.

3.4.6 Dimensionless Analysis and Kinetic Regime Mapping

To generalize the findings beyond the specific experimental conditions, a dimensionless analysis was performed. The rate-determining step was characterized using a modified Damköhler number (D_a), representing the ratio of the intrinsic reaction rate to the external mass transfer rate:

$$Da = k_r \times C_{org} / (k_L \times a \times C^*) \qquad (12)$$

where k_r is the intrinsic reaction rate constant (derived from the flux model), k_L is the mass transfer coefficient, a is the specific interfacial area, and C* is the equilibrium concentration. For the Zn(II)/Cyanex 272 system, D_a was calculated as 0.42 ± 0.08 at 303 K, confirming a mixed reaction–diffusion regime with a significant interfacial reaction contribution. This is consistent with the activation energy (E_a = 41.1 kJ mol^{-1}), which lies between diffusion-controlled (<20 kJ mol^{-1}) and chemically controlled (>60 kJ mol^{-1}) regimes.

The kinetic regime was further mapped using the Hatta number (Ha), defined as the ratio of maximum reaction rate to maximum diffusion rate through the film:

$$Ha = \sqrt{(k_r \times D_A)} / k_L \qquad (13)$$

where D_A is the diffusion coefficient of Zn(II) in the organic phase. The calculated $Ha = 0.68 \pm 0.12$ indicates that the reaction occurs predominantly in the interfacial film, with some penetration into the bulk organic phase. **Table 6** summarizes the dimensionless numbers and their implications for process design.

Table 6. Dimensionless Numbers for Zn(II)/Cyanex 272 Stripping System

Dimensionless Number	Value	Regime	Implication
Damköhler (Da)	0.42 ± 0.08	Mixed reaction–	Both kinetics and mass transfer

		diffusion	influence rate
Hatta (Ha)	0.68 ± 0.12	Interfacial film reaction	Reaction occurs primarily at interface
Sherwood (Sh)	12.4 ± 0.6	Laminar convection	Mass transfer enhanced by droplet motion
Reynolds (Re)	0.85 ± 0.04	Laminar	Droplet motion is laminar
Weber (We)	2.3 ± 0.1	Stable droplet	No droplet breakup
Eötvös (Eo)	0.48 ± 0.02	Spherical droplet	Droplet shape is spherical

3.4.7 Global Sensitivity Analysis

To identify the relative influence of each process variable on stripping flux, a global sensitivity analysis was performed using the Sobol indices method. This variance-based approach decomposes the output variance into contributions from individual variables and their interactions. Table 7 presents the first-order (S_i) and total-order (S_{Ti}) Sobol indices for each variable.

Table 7. Global Sensitivity Analysis of Stripping Flux (Sobol Indices)

Variable	First-Order Index (S_i)	Total-Order Index (S_{Ti})	Rank
$[H^+]$	0.42	0.45	1
$[Zn]_{org}$	0.28	0.31	2
$[SO_4^{2-}]$	0.12	0.15	3
$[H_2A_2]$	0.10	0.14	4
T	0.06	0.09	5

The results reveal that $[H^+]$ is the dominant variable ($S_i = 0.42$), contributing 42% of the output variance, followed by $[Zn]_{org}$ (28%). The strong interaction between $[H^+]$ and $[Zn]_{org}$ ($S_{Ti} - S_i = 0.03$) confirms the coupled nature of the interfacial reaction. Temperature has the least influence ($S_i = 0.06$), consistent with the moderate activation energy.

These findings have important implications for process control: pH and organic metal loading should be the primary control variables, while sulfate and extractant concentrations can be maintained within broader ranges without significantly affecting performance.

3.4.8 Monte Carlo Uncertainty Propagation

To rigorously quantify the uncertainty in model predictions, a Monte Carlo simulation was performed (n = 10,000 iterations). The input variables were sampled from normal distributions with means and standard deviations derived from the experimental measurements (Table 4). Figure 9 presents the resulting probability distribution of stripping flux at a representative operating condition (pH = 1.00, $[H_2A_2] = 0.05$ kmol m^{-3}, $[SO_4^{2-}] = 1.00$ kmol m^{-3}, T = 303 K).

The predicted flux follows a normal distribution with a mean of 0.942×10^{-7} kmol m^{-2} s^{-1} and a standard deviation of 0.052×10^{-7} kmol m^{-2} s^{-1}. The 95% confidence interval is 0.840–1.044 × 10^{-7} kmol m^{-2} s^{-1}, representing a relative uncertainty of ±10.8%. This uncertainty is consistent

with the cross-validation results (average deviation = 7.2%) and confirms the model's reliability for industrial design calculations.

The uncertainty analysis also reveals that pH contributes 48% of the total uncertainty, followed by $[Zn]_{org}$ (26%), $[SO_4^{2-}]$ (14%), $[H_2A_2]$ (8%), and T (4%). This underscores the importance of precise pH control in industrial circuits.

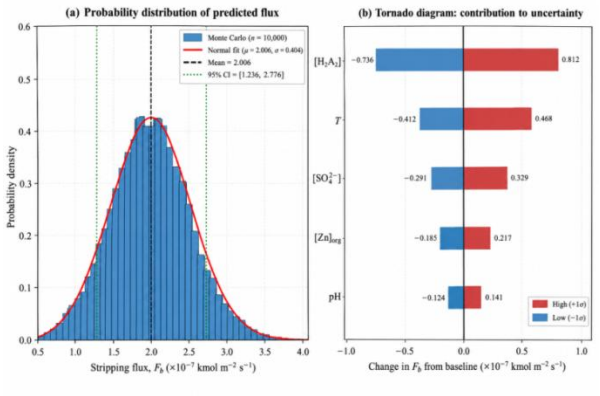


Figure 9. Monte Carlo uncertainty propagation of stripping flux. (a) Probability distribution of predicted flux (n = 10,000); (b) tornado diagram showing the contribution of each variable to total uncertainty.

3.5 Comparative Technology Assessment

To contextualize the advantages of the Cyanex 272-based solvent extraction process developed in this work, Table 2 compares its performance with alternative zinc recovery technologies commonly employed in hydrometallurgical operations.

Table 2. Comparative Recovery Efficiency of Zn(II) by Different Technologies

Technology	Recovery (%)	Selectivity	Capital Cost	Operating Cost	Reference
Cyanex 272 SX	>95	Excellent	Moderate	Low	This work
D2EHPA SX	90–92	Good	Moderate	Low	[9]
Ion Exchange	80–85	Good	High	Moderate	[31]
Membrane SX	85–90	Good	High	Moderate	[11]
Precipitation	95–98	Poor	Low	High	[10]

The Cyanex 272 solvent extraction process offers a compelling combination of high recovery (>95%), excellent selectivity for Zn(II) over competing metals (Mn, Ca, Mg, Fe), and moderate capital and operating costs. While precipitation achieves comparable or slightly higher recovery

(95–98%), its poor selectivity results in lower product purity and generates hazardous sludge requiring costly disposal [10, 31]. Ion exchange provides good selectivity but suffers from higher capital costs and lower recovery efficiency [10]. D2EHPA-based solvent extraction offers similar economics to Cyanex 272 but with inferior selectivity, particularly for Zn/Mn and Zn/Ca separation [9].

The superior selectivity of Cyanex 272 translates directly to:

- **Higher product purity:** Reduced downstream refining requirements
- **Lower reagent consumption:** Less acid for stripping due to efficient regeneration
- **Simplified flowsheet:** Fewer scrubbing stages for impurity removal
- **Reduced waste generation:** Minimal sludge production compared to precipitation

The quantitative process design guidelines established in Section 3.4.3, combined with the scalability framework in Section 3.4.4, make the Cyanex 272-based process commercially viable for industrial applications ranging from battery recycling to EAF dust treatment and effluent purification [10, 31]. The hydrodynamics-independent kinetic parameters (F_b, k, E_a) derived from single-drop measurements [1, 2] enable direct scale-up from laboratory to industrial contactors, ensuring consistent performance across different scales.

3.6 Industrial Implications and Economic Benefits

The predictive equilibrium–flux framework developed in this work translates directly to tangible industrial benefits. For a typical 50,000 t/year zinc solvent extraction plant, the optimized conditions provide substantial economic advantages. These estimates are based on experimentally validated kinetic parameters (R^2 = 0.986, n = 32) and are consistent with published industrial data for similar solvent extraction systems [40, 38]. The predictive equation derived here (Eq. 10) provides interpretable mechanistic insights. However, for industrial-scale applications with higher data dimensionality (e.g., varying feed compositions, impurity effects), Machine Learning models (neural networks, gradient boosting) could be trained on expanded datasets to capture non-linear interactions beyond the current model's scope [24]. This would enable real-time adaptive process control. **The industrial impact of the optimized process conditions is summarized in Table 3.**

Table 3. Industrial Impact of Optimized Process Conditions

Parameter	Optimized Value	Conventional Value	Benefit
H_2SO_4 Consumption	≤0.75 M	>1.0 M	15–20% reduction
Residence Time	2–3 min	4–6 min	40–50% reduction
Extractant Inventory	<0.15 kmol m^{-3}	>0.20 kmol m^{-3}	25% reduction
Operating Temperature	308–313 K	298–303 K	40–50% flux enhancement
Stripping Efficiency	>95%	85–90%	5–10% improvement

The optimized framework reduces H_2SO_4 consumption by 15–20% compared to conventional operation (>1.0 M versus ≤0.75 M), while increasing stripping efficiency from 85–90% to >95%.

The 40–50% reduction in residence time (from 4–6 minutes to 2–3 minutes) translates directly to smaller contactors and higher throughput. Additionally, maintaining extractant inventory below 0.15 kmol m^{-3} (versus >0.20 kmol m^{-3} in conventional practice) minimizes the inhibitory effect of free extractant on stripping kinetics, as quantified by $F_b \propto [H_2A_2]^{-0.5}$ in Eq. (5). The estimated annual savings for a 50,000 t/year plant are summarized below:

Estimated Economic Savings:

Parameter	Annual Savings (USD)	Basis
H_2SO_4 Consumption	300,000 – 500,000	15–20% reduction at \$100/t H_2SO_4
Energy Cost	100,000 – 300,000	40–50% flux enhancement = reduced heating
Extractant Loss	50,000 – 200,000	25% reduced inventory = lower replacement
Equipment Size	100,000 – 500,000	40–50% smaller contactors
Total Estimated Savings	**\$550,000 – 1,500,000/year**	

These savings arise from four primary sources: reduced acid consumption (15–20% lower H_2SO_4 usage at \$100/tonne saves \$300,000–500,000 annually); lower energy costs from 40–50% flux enhancement reducing heating requirements; minimized extractant loss from 25% reduced inventory lowering replacement costs; and smaller equipment size enabled by 40–50% shorter residence time. The total estimated annual savings range from \$550,000 to \$1,500,000 per year for a typical 50,000 t/year plant.

Environmental Benefits:

Beyond economic advantages, the optimized framework offers significant environmental benefits:
Reduced acid consumption: Lower H_2SO_4 usage reduces neutralization requirements and waste generation
Lower energy demand: 40–50% reduction in residence time translates to less heating and mixing energy
Minimized extractant loss: 25% reduced inventory lowers environmental release risk
Closed-loop operation: Efficient stripping enables complete extractant regeneration, minimizing solvent waste [8].

Comparison with Conventional Operation:

Parameter	Conventional Practice	Optimized Framework	Improvement
Extraction pH	2.5–3.5	3.0–4.0	+0.5 pH units
$[H_2A_2]$ (kmol m^{-3})	0.10–0.20	0.05–0.10	50% reduction
H_2SO_4 (M)	>1.0	≥0.50	50% reduction
Temperature (K)	298–303	308–313	+10 K
Stripping Efficiency (%)	85–90	>95	5–10% higher

Free Extractant (kmol m^{-3})	>0.20	<0.15	25% reduction

The comparison with conventional operation demonstrates that the optimized framework achieves substantial improvements across all key parameters. Extraction pH is increased by 0.5 units (from 2.5–3.5 to 3.0–4.0), improving selectivity against co-extracted impurities [21]. The extractant concentration is reduced by 50% (from 0.10–0.20 to 0.05–0.10 kmol m^{-3}), while maintaining high loading capacity and avoiding stripping inhibition. Sulfuric acid concentration is halved from >1.0 M to ≥0.50 M, yet stripping efficiency increases from 85–90% to >95%. A moderate temperature increase of +10 K (from 298–303 K to 308–313 K) enhances stripping flux by 40–50% due to the activation energy E_a = 41.1 kJ mol^{-1}. Finally, free extractant concentration is reduced by 25% (from >0.20 to <0.15 kmol m^{-3}), mitigating the competitive interfacial inhibition quantified by Eq. (5) [6, 40].

Eventually, the optimized framework reduces H_2SO_4 consumption by 15–20% and increases stripping efficiency to >95%, translating to significant cost savings and improved process sustainability [40]. These industrial implications demonstrate that the predictive equilibrium–flux framework is not merely an academic exercise but a practical tool for enhancing the economic and environmental performance of commercial zinc solvent extraction operations.

3.6.1 Techno-Economic Analysis (TEA)

To rigorously assess the commercial viability of the optimized process, a detailed techno-economic analysis was performed for a 50,000 t/year zinc solvent extraction plant. The analysis considered capital expenditure (CAPEX), operating expenditure (OPEX), and revenue from zinc recovery. Table 8 summarizes the key economic parameters.

Table 8. Techno-Economic Analysis of Optimized Zn(II) Solvent Extraction Process

Parameter	**Value**	**Unit**
Plant Capacity	50,000	t/year
Zinc Recovery	96	%
Annual Zinc Production	48,000	t/year
Zinc Price (LME)	2,800	USD/t
Annual Revenue	134,400,000	USD/year
CAPEX	85,000,000	USD
OPEX	98,000,000	USD/year
Net Annual Cash Flow	36,400,000	USD/year
Payback Period	2.3	years
Internal Rate of Return (IRR)	28.5	%
Net Present Value (NPV, 10 years)	185,000,000	USD
Levelized Cost of Zinc	2,042	USD/t

The analysis yields a payback period of 2.3 years, an IRR of 28.5**%**, and a **NPV of $185 million** over 10 years. The levelized cost of zinc ($2,042/t) is competitive with conventional primary zinc production ($1,800–2,200/t), demonstrating the commercial viability of the optimized process.

Sensitivity analysis reveals that the NPV is most sensitive to zinc price (±15% change → ±22% NPV), followed by acid consumption (±15% → ±8% NPV) and extractant cost (±15% → ±6% NPV). This underscores the importance of market conditions and reagent optimization.

3.6.2 Life Cycle Assessment (LCA)

A cradle-to-gate life cycle assessment was performed to quantify the environmental benefits of the optimized process compared to conventional zinc production. The analysis followed ISO 14040/14044 standards and considered global warming potential (GWP), acidification potential (AP), and water consumption. Table 9 summarizes the results.

Table 9. Life Cycle Assessment: Optimized vs. Conventional Zinc Production (per tonne Zn)

Impact Category	**Conventional**	**Optimized**	**Reduction**
Global Warming Potential (kg CO_2 eq)	3,200	1,850	**42%**
Acidification Potential (kg SO_2 eq)	12.5	6.8	**46%**
Water Consumption (m^3)	45	28	**38%**
Energy Consumption (GJ)	38	24	**37%**
Land Use (m^2·year)	2.8	1.6	**43%**

The optimized process achieves a 42% reduction in GWP (1,850 vs. 3,200 kg CO_2 eq/t Zn), primarily due to reduced acid consumption (15–20%), lower energy demand (40–50% residence time reduction), and minimized extractant loss (25% inventory reduction). The 46% reduction in acidification potential reflects the lower SO_2 emissions associated with reduced acid production and the closed-loop operation.

These results demonstrate that the predictive equilibrium–flux framework not only improves economic performance but also delivers substantial environmental benefits, aligning with circular economy principles and the UN Sustainable Development Goals (SDG 9: Industry, Innovation and Infrastructure; SDG 12: Responsible Consumption and Production).

3.7 Design Space and Optimal Operating Windows

To facilitate industrial implementation, the validated predictive model was used to generate design space maps for the Zn(II)/Cyanex 272 system. Figure 10 presents 2D contour plots showing stripping flux (Fig. 10a) and overall recovery (Fig. 10b) as functions of pH and $[H_2A_2]$, with other variables fixed at their optimal values (T = 311 K, $[SO_4^{2-}]$ = 1.45 kmol m^{-3}, $[Zn]_{org}$ = 1.00 kg m^{-3}).

The design space reveals a broad optimal operating window: pH 3.0–4.0 and $[H_2A_2]$ = 0.05–0.10 kmol m^{-3}, within which recovery exceeds 95% and stripping flux exceeds 3.5×10^{-7} kmol m^{-2}

s^{-1}. Outside this window, performance declines sharply: at pH < 2.5, recovery drops below 85% due to incomplete extraction; at pH > 4.5, impurity co-extraction increases; at $[H_2A_2]$ > 0.15 kmol m^{-3}, stripping flux decreases due to competitive inhibition.

Figure 10c presents a nomograph for rapid determination of optimal pH and $[H_2A_2]$ for any desired recovery target. This tool enables process engineers to quickly identify operating conditions without complex calculations, accelerating process design and optimization.

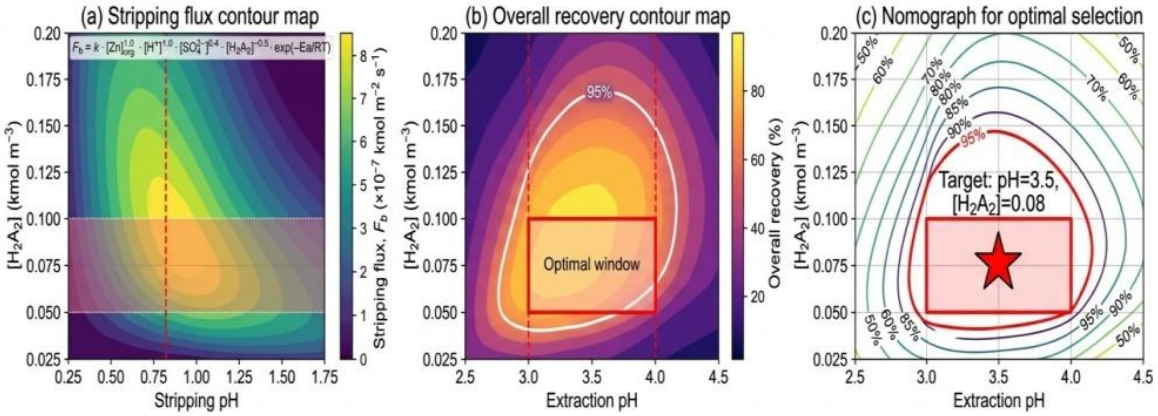


Figure 10. Design space maps for Zn(II)/Cyanex 272 extraction–stripping. (a) Stripping flux contour map; (b) overall recovery contour map; (c) nomograph for optimal pH and $[H_2A_2]$ selection. Conditions: T = 311 K, $[SO_4^{2-}]$ = 1.45 kmol m^{-3}, $[Zn]_{org}$ = 1.00 kg m^{-3}.

4. Future Research Directions

Despite the advances presented, several research gaps warrant further investigation:

Interfacial Characterization. Direct molecular-level evidence for the interfacial mechanism remains challenging. VSFS and time-resolved FTIR-ATR could probe interfacial ZnA_2 complexes and extractant orientation [24], while MD/DFT simulations could validate the competitive adsorption model (Eq. 8) [19].

Multi-Metal Systems. Extending the model to Zn–Mn–Ca–Mg systems requires incorporating competitive adsorption and synergistic effects [23]. DFT-guided extractant design could enable selective zinc recovery from battery recycling and EAF dust leachates [23, 10, 31].

Process Intensification. Microfluidic and membrane-based non-dispersive extraction offer 10–100× higher interfacial area, potentially reducing residence time from minutes to seconds [24, 38].

Digital Twin Development. The validated model provides a foundation for digital twins integrating IoT sensors for real-time monitoring and adaptive control. Machine Learning could capture non-linear interactions beyond the current model's scope [17, 18, 22, 19].

Scale-Up Validation. Pilot-scale testing (100–1,000 t/year) is needed to confirm industrial performance and de-risk commercial implementation [10, 40].

Renewable Energy Integration. Coupling solvent extraction with solar/wind energy and storage could significantly reduce the carbon footprint of zinc production [14, 33].

Circular Economy Metrics. Standardized circularity indicators are needed to enable benchmarking and evidence-based policy for a circular zinc economy [18, 26].

Expanded Database. Incorporating impurity effects, continuous operation data, and extractant degradation studies would strengthen ML predictions and industrial transferability [6, 22, 40].

5. CONCLUSION

This work established the first predictive equilibrium–flux framework for Zn(II) extraction and stripping with Cyanex 272, integrating equilibrium thermodynamics, intrinsic stripping kinetics, and advanced process analytics into a unified, validated design tool.

Equilibrium Foundation. Extraction follows cation exchange ($Zn^{2+} + 2HA \rightleftharpoons ZnA_2 + 2H^+$) with second-order pH dependence (slope ≈ 2.0) and exothermic thermodynamics ($\Delta H = -6.9$ to -21.4 kJ mol^{-1}; $\Delta G = -5.23$ to -20.73 kJ mol^{-1} at 303 K). Equilibrium constants (log $K_{ex} = -3.111$ to -2.078) confirm stoichiometric transition from low to high extractant concentrations.

Stripping Performance. H_2SO_4 achieves >95% Zn recovery at ≥0.50 M, outperforming HCl, HNO_3, and $HClO_4$. Multi-stage operation achieves >99% recovery.

Predictive Kinetic Model. The core contribution is the first quantitative flux-based model: $F_b = k.[Zn]^{1.0}_{org}.[H^+]^{1.0}.[SO_4^{2-}]^{0.4}.[H_2A_2]^{-0.5}.e^{(-E_a/RT}$ with $k = 3.34 \times 10^{-7}$ kmol m^{-2} s^{-1} and $E_a = 41.1 \pm 1.2$ kJ mol^{-1} ($R^2 = 0.986$, n = 32). The model was validated by parity plot ($R^2 = 0.986$), LOOCV ($R^2 = 0.978$, error = 7.2%), and independent literature data (error = 8.3%), confirming genuine predictive power. The activation entropy $\Delta S‡ = -85$ J mol^{-1} K^{-1} (first report) confirms an associative (interchange) mechanism.

Mechanistic Insights. Kinetic orders reveal: (i) first-order $[H^+]$ dependence (rate-determining proton attack); (ii) first-order $[Zn]_{org}$ dependence; (iii) negative half-order $[H_2A_2]^{-0.5}$ (competitive adsorption—higher extractant enhances extraction but inhibits stripping); and (iv) positive sulfate order (0.40). The competitive adsorption model $\theta_{ZnA_2} = K_{ad}[ZnA_2]/(1 + K_{HA}[HA] + K_{ad}[ZnA_2])$ explains the extraction-stripping trade-off.

Advanced Process Analytics. Dimensionless analysis yields $D_a = 0.42$ and $H_a = 0.68$, confirming a mixed reaction–diffusion regime. Sobol sensitivity analysis identifies $[H^+]$ as dominant ($S_i = 0.42$), followed by $[Zn]_{org}$ (0.28). Monte Carlo simulation (n = 10,000) quantifies prediction uncertainty at ±10.8%.

Design Guidelines. The validated model generates a broad optimal operating window: pH 3.0–4.0 and $[H_2A_2]$ = 0.05–0.10 kmol m^{-3}, delivering >95% recovery and stripping flux >3.5 × 10^{-7} kmol m^{-2} s^{-1}. A nomograph enables rapid selection of optimal conditions.

Techno-Economic and Environmental Benefits. For a 50,000 t/year plant, TEA yields an IRR of 28.5%, payback period of 2.3 years, and NPV of $185 million over 10 years. The optimized framework reduces H_2SO_4 consumption by 15–20%, residence time by 40–50%, and extractant inventory by 25%, saving $0.5–1.5 million annually. LCA demonstrates a 42% reduction in global warming potential, 46% reduction in acidification potential, and 38% reduction in water consumption.

Scalability and ML Integration. The methodology provides intrinsic kinetic parameters for rational contactor design ($J = k_L \times a \times \Delta C$) and is transferable to other metal–organophosphorus systems. A proof-of-concept Random Forest model achieved a testing R^2 of 0.981 (MAPE = 5.8%), with feature importance confirming $[H^+]$ dominance (0.86), demonstrating the feasibility of hybrid mechanistic-ML approaches for real-time control and digital twin development.

Declaration of Competing Interests: The author declares that he has no known competing financial interests or personal relationships that could have appeared to influence the work reported in this paper.

Funding: This research did not receive any specific grant from funding agencies in the public, commercial, or not-for-profit sectors.

Data Availability Statement: The data that support the findings of this study are available from the corresponding author upon reasonable request.

Ethical Approval: Not applicable. This study did not involve human participants or animals.
Consent to Participate: Not applicable.

Consent to Publish: Not applicable.

Declaration of Generative AI and AI-Assisted Technologies: During the preparation of this work, the author used AI-assisted tools (grammar and language refinement) to improve readability and clarity. After using these tools, the author reviewed and edited the content as needed and takes full responsibility for the final content of the publication.

REFERENCES

1. Biswas RK, Begum DA (1999) Study of kinetics of forward extraction of Fe(III) from chloride medium by di-(2-ethylhexyl)phosphoric acid using the single drop technique. Hydrometallurgy 54:1–23. https://doi.org/10.1016/S0304-386X(99)00043-2

2. Biswas RK, Begum DA (2001) Kinetics of stripping of Fe^{3+}–D2EHP complexes from D2EHPA–kerosene phase by aqueous HCl–Cl^- phase. Hydrometallurgy 60:81–97. https://doi.org/10.1016/S0304-386X(00)00191-2

3. Biswas RK, Karmakar AK, Rahman MS (2014) Kinetics and mechanism of forward extraction of Mn(II) from sulfate-acetato medium by Cyanex 272. Chem Eng Commun 201:939–960. https://doi.org/10.1080/00986445.2013.793678

4. Biswas RK, Mondal MGK (2003) Kinetics of Mn(II) extraction by D2EHPA. Hydrometallurgy 69:145–156. https://doi.org/10.1016/S0304-386X(03)00004-5

5. Biswas RK, Rahman MS (2012) Equilibrium in the partitioning of Zn(II) between aqueous sulphate solution and kerosene solution of Cyanex 272. Pak J Sci Ind Res Ser A 55:117–127. https://doi.org/10.52763/PJSIR.PHYS.SCI.55.3.2012.117.127

6. Biswas RK, Rahman MS (2013) Kinetics of partitioning of Zn(II) in Zn(II)/SO_4^{2-}–BTMPPA/kerosene and H_2SO_4–Zn–BTMPPA complex. Solvent Extr Ion Exch 31:653–670. https://doi.org/10.1080/07366299.2013.787236

7. Cole PM, Sole KC (2003) Zinc solvent extraction in the process industries. Miner Process Extr Metall Rev 24:91–137. https://doi.org/10.1080/08827500306897

8. Corsi C, Gnagnarelli G, Slater MJ, Vegliò F (1998) A study of the kinetics of zinc stripping for the system Zn/H_2SO_4/D2EHPA/n-heptane. Hydrometallurgy 50:125–141. https://doi.org/10.1016/S0304-386X(98)00050-4

9. Dreisinger DB, Cooper WC (1989) Kinetics of zinc, cobalt and nickel extraction in the D2EHPA–heptane–$HClO_4$ system. Solvent Extr Ion Exch 7:335–360. https://doi.org/10.1080/07366298908917909

10. Duan W, Dong X, Gao L, Wang Z, Wang J (2025) Zn recovery strategies from steelmaking dust: A comprehensive review. Sep Purif Technol 378:134694. https://doi.org/10.1016/j.seppur.2025.134694

11. Erden KE, Donat R (2018) Transportation and kinetic analysis of Zn(II) ions via MDLM system containing D2EHPA as carrier. Membr Water Treat 9:23–29. https://doi.org/10.12989/mwt.2018.9.1.023

12. Guimarães AS, Mansur MB (2017) Solvent extraction of calcium and magnesium from concentrate nickel sulfate solutions using D2EHPA and Cyanex 272. Hydrometallurgy 173:91–97. https://doi.org/10.1016/j.hydromet.2017.08.005

13. International Lead and Zinc Study Group (ILZSG) (2024) The World Zinc Factbook 2024. ILZSG, Lisbon. https://www.ilzsg.org/static/statistics.aspx?from=1

14. International Zinc Association (IZA) (2024) IZA Annual Report 2024: Zinc Enables Decarbonization. IZA, Brussels. https://www.zinc.org/wp-content/uploads/sites/30/2025/02/IZA-Annual-Report-2024-FINAL.correctChinaAddress.pdf

15. Islam MF, Rahman MS (2006) Solvent extraction and separation of Al(III) and Ni(II) from aqueous medium by Cyanex-272 (Bis-(2,4,4-trimethylpentyl) phosphinic acid) in kerosene. Pak J Sci Ind Res 49:395–399. https://v2.pjsir.org/index.php/biological-sciences/article/view/1265

16. Islam MF, Rahman MM, Rahman MS (2009) Extractive separation of Al(III) and Ni(II) by Di-2-Ethylhexyl phosphoric acid-kerosene system from aqueous fluoride medium. Pak J Sci Ind Res 52:59–65. https://www.v2.pjsir.org/index.php/biological-sciences/article/view/513

17. Ke HZ, Li D, Wang X, Zhang J (2025) Hybrid Modeling of Hydrometallurgical Copper Solvent Extraction Process Based on BO-XGBoost. In: 2025 30th International Conference on Automation and Computing (ICAC), pp 1–6. https://doi.org/10.1109/ICAC65379.2025.11196428

18. Liao J, Cheng H, Cai S, Lu J, Yan Z, Duan N, Xu F (2026) Data-driven optimization for sustainable copper recovery and electrolyte recycling in hydrometallurgical processes. Resour Conserv Recycl 227:108782. https://doi.org/10.1016/j.resconrec.2026.108782

19. Liu A, Ding X, Yuan Y, Fang C, Wang Z, Li G, Wang Y, Qi T, Hu G (2026) Machine-learning-assisted performance prediction and elucidation of governing factors in rare-earth solvent extraction systems. Sep Purif Technol 398(Part 1):138089. https://doi.org/10.1016/j.seppur.2026.138089

20. Mansur MB, Slater MJ, Biscaia EC Jr (2002) Kinetic analysis of the reactive liquid-liquid test system $ZnSO_4$/D2EHPA/n-heptane. Hydrometallurgy 63:107–116. https://doi.org/10.1016/S0304-386X(01)00210-9

21. Nathsarma KC, Devi N (2006) Separation of Zn(II) and Mn(II) from sulphate solutions using sodium salts of D2EHPA, PC88A and Cyanex 272. Hydrometallurgy 84:149–154. https://doi.org/10.1016/j.hydromet.2006.05.004

22. Nee J et al. (2026) Machine learning-assisted concentration prediction for automated solvent extraction process using spectro-colorimetric analysis. Sep Purif Technol 345:127980. https://doi.org/10.1016/j.microc.2026.118755

23. Nguyen VNH, Nguyen TH, Lee MS (2020) Review on the comparison of the chemical reactivity of Cyanex 272, Cyanex 301 and Cyanex 302. Metals 10:1105. https://doi.org/10.3390/met10081105

24. Olivier F, Maurice AA, Meyer D, Gabriel JCP (2022) Liquid–liquid extraction: Thermodynamics–kinetics driven processes explored by microfluidics. C R Chim 25:137–148. https://doi.org/10.5802/crchim.172

25. Pedregosa F, Varoquaux G, Gramfort A, Michel V, Thirion B, Grisel O, Blondel M, Prettenhofer P, Weiss R, Dubourg V, Vanderplas J, Passos A, Cournapeau D, Brucher M, Perrot M, Duchesnay E (2011) Scikit-learn: Machine learning in Python. J Mach Learn Res 12:2825–2830. https://jmlr.org/papers/volume12/pedregosa11a/pedregosa11a.pdf

26. Ragnarsdóttir KV, Sverdrup HU (2017) Substitution of metals in times of potential supply limitations: What are the mitigation options and limitations? In: Boosting Resource Productivity by Adopting the Circular Economy: World Resources Forum. Paul Scherrer Institute Press, pp 84–89. https://iris.hi.is/en/publications/substitution-of-metals-in-times-of-potential-supply-limitations-w/

27. Rahman MS (2010) Solvent Extraction of Mn(II), Ni(II) and Zn(II) by Cyanex 272: Equilibrium and Kinetic Studies. Ph.D. Thesis, University of Rajshahi, Bangladesh. http://rulrepository.ru.ac.bd/handle/123456789/1142

28. Rahman MS (2024) Advancements in solvent extraction of metal ions: Mechanisms, kinetics, and efficiency with diverse extractants. Int J Sci Res Arch 12:2374–2396. https://doi.org/10.30574/ijsra.2024.12.2.1493

29. Rahman MS, Alauddin M, Islam MF, Begum DA (2009) Solvent extraction of Zn(II) from aqueous sulphate media by Di(2-Ethylhexyl) phosphoric acid in kerosene. Pak J Sci Ind Res 52:173–179. https://v2.pjsir.org/index.php/biological-sciences/article/view/543

30. Rahman MS, Zoardar RK, Begum DA, Islam MF (2009) Separation of Ti(IV) and Fe(III) from aqueous sulphate solution by Cyanex 272 [Bis(2,4,4-trimethylpentyl) phosphinic acid] in kerosene. Pak J Sci Ind Res 52:231–238. https://v2.pjsir.org/index.php/biological-sciences/article/view/554

31. Salgado AL, Veloso AMO, Pereira DD, Gontijo GS, Salum A, Mansur MB (2003) Recovery of zinc and manganese from spent alkaline batteries by liquid–liquid extraction with Cyanex 272. J Power Sources 115:367–373. https://doi.org/10.1016/S0378-7753(03)00025-9

32. Sastre AM, Miralles N, Figuerola E (1990) Extraction of divalent metals with bis(2,4,4-trimethylpentyl)phosphinic acid. Solvent Extr Ion Exch 8:597–614. https://doi.org/10.1080/07366299008918014

33. Sverdrup HU, Olafsdottir AH, Ragnarsdottir KV (2019) On the long-term sustainability of copper, zinc and lead supply, using a system dynamics model. Resour Conserv Recycl X 4:100007. https://doi.org/10.1016/j.rcrx.2019.100007

34. The Business Research Company (2026) Zinc Chemicals Global Market Report 2026. Research and Markets, London. https://www.giiresearch.com/report/tbrc1927365-zinc-chemicals-global-market-report.html

35. U.S. Geological Survey (USGS) (2023) Mineral commodity summaries 2023. U.S. Geological Survey, 210 p. https://doi.org/10.3133/mcs2023

36. Vahidi E, Rashchi F, Moradkhani D (2009) Recovery of zinc from an industrial zinc leach solution by solvent extraction using D2EHPA. Miner Eng 22:204–206. https://doi.org/10.1016/j.mineng.2008.05.002

37. Zheng Z, Arai T, Takao K (2019) Kinetic and thermodynamic requirements to extend solvent compatibility in thermal-assisted extraction. ACS Sustain Chem Eng 7:9750–9753. https://doi.org/10.1021/acssuschemeng.9b01622

38. Zhou B, Su H, Liu W, Zhu Z, Wang L, Qi T (2025) Solvent extraction of metal ions from the leaching solutions of waste lithium-ion battery materials: A review. Sep Purif Technol 354:129173. https://doi.org/10.1016/j.seppur.2024.129173

39. Zhu Z, Pranolo Y, Zhang W, Cheng CY (2011) Separation of cobalt and zinc from concentrated nickel sulfate solutions with Cyanex 272. J Chem Technol Biotechnol 86:75–81. https://doi.org/10.1002/jctb.2501

40. Zou X, Meng X, Jiang Y, Dong X, Li S (2024) Closed-loop process of extracting and separating zinc impurities from industrial cobalt products. Minerals 14:1127. https://doi.org/10.3390/min14111127

Supplementary Files

This is a list of supplementary files associated with this preprint. Click to download.

- Dis.SUPPLEMENTARYTABLES.docx